Proceedings of SMASIS08
ASME Conference on Smart Materials, Adaptive Structures and Intelligent Systems
October 28-30, 2008, Ellicott City, Maryland, USA

SMASIS2008-475

ACOUSTIC SENSOR WITH PVDF MICRO-PILLARS AND PATTERNED ELECTRODES

Jian Xu
Smart Vehicle Concepts Center
Department of Mechanical Engineering
The Ohio State University
Columbus, OH 43210
Email: xu.212@osu.edu

Marcelo J. Dapino*
Smart Vehicle Concepts Center
Department of Mechanical Engineering
The Ohio State University
Columbus, OH 43210
Email: dapino.1@osu.edu

Daniel Gallego Perez
Department of Biomedical Engineering
The Ohio State University
Columbus, OH 43210
Email: gallego-perez.2@osu.edu

Derek Hansford
Department of Biomedical Engineering
The Ohio State University
Columbus, OH 43210
Email: hansford.4@osu.edu

ABSTRACT

This paper addresses the design and theoretical analysis of a new type of millimeter-size acoustic sensor that uses Polyvinylidene Fluoride (PVDF) micro-pillars and patterned electrodes. The sensor has the potential to achieve 100x the sensitivity of existing commercial sensors in combination with a dynamic range of 181dB and a frequency bandwidth of at least 100 kHz. A constrained optimization algorithm has been developed as a function of geometric parameters (sensor footprint, diameter and height of the micro-pillars, gap between pillar edges, number of pillars) and electrical parameters of the sensor and conditioning amplifier.

INTRODUCTION

The piezoelectric polymer Polyvinylidene Fluoride (PVDF) has been widely used in sensor development [1]. Sensors based on PVDF piezo-electric polymers have many advantages, such as wide frequency range (0.001Hz to 10^9 Hz), superior dynamic range (10^{-4} to 10^9 Pa), high elastic compliance, high mechanical strength and impact resistance, and low acoustic impedance. PVDF polymers can generate 10 to 25 times higher voltage output than piezoceramic materials for the same force input and are quite stable as they can resist moisture, most chemicals, oxidants, and intense ultraviolet and nuclear radiation.

Sensors based on PVDF film are attractive due to their high sensitivity and low cost. For example, a PVDF film pressure sensor is used for in-sleep cardiorespiratory monitoring [2]. Uncooled infrared (IR) sensors using PVDF thin film are used to detect temperature changes from low levels of incident IR radiation [3].

We have developed models and conducted characterization experiments on PVDF film-based sensors. The sensors were modeled in rods, beams, hemispherical and cylindrical shapes (following work in [4] and [5]) and design parameters were selected to detect the acoustic frequency range. Compared to flat film, the cylindrical curvature has a higher sensitivity. We consequently built a microphone based on the cylindrical curvature model with a footprint of 10mm x 10mm x 6mm (R x L x W) and set up an experiment to detect acoustic signals. By analyzing the results of FFT and frequency response, we found that the sensitivity of our microphone is overall equivalent to that of a typical commercial sound level meter in low and high frequency ranges, despite its design not being optimal. This result motivates the development of PVDF sensor designs with yet superior sensitivity and miniature dimensions. The objective of this paper is to analytically show that PVDF sensors based on micro-pillar arrays and patterned electrodes exhibit much higher sensitivity than both commercial PVDF film sensors and micro-pillar arrays with full electrodes, while exhibiting an equally broad frequency bandwidth.

MEMS technology has traditionally been focused on silicon based fabrication techniques. With the development of sacrificial layer micromolding (SLaM) and patterned substrate

* Address all correspondence to this author.

micromolding (PSM), the micro-fabrication of polymer microstructures is becoming increasingly promising [6]. Two soft lithography fabrication techniques will be considered in future work for fabricating our acoustic sensor [7].

NOMENCLATURE

M	number of pillars in *x*-direction
N	number of pillars in *y*-direction
h	pillar height
d	pillar diameter
g_1	gap between pillars in *x*-direction
g_2	gap between pillars in *y*-direction
g_{33}	piezo stress constant
ε_r	relative permittivity of PVDF
ε	permittivity of PVDF
ε_o	permittivity of air
E	Young's modulus of PVDF
ρ_0	mass density of PVDF

SENSOR DESIGN

Geometry Design and Sensitivity Analysis

We propose a new acoustic sensor based on PVDF pillar elements with patterned electrodes. Figure 1 depicts one possible sensor configuration of a PVDF micro-pillar array. A flat electrode is placed underneath the array, and a patterned electrode is placed on top of the pillars in such a way that each pillar is activated by a single round electrode. The pillars are connected in electrical parallel.

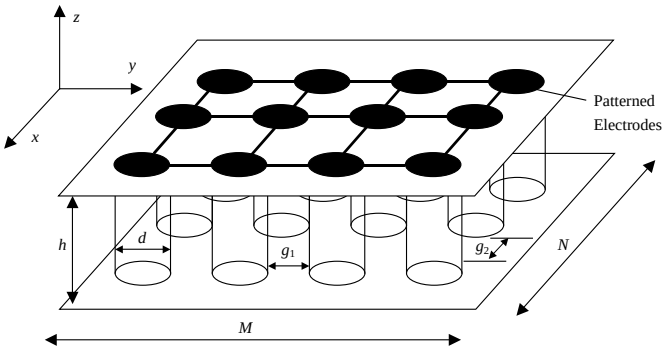

Figure 1. Schematic diagram of PVDF micro-pillar sensor based on patterned electrodes.

For a given sensing area and input pressure, the introduction of air gaps between the micro-pillars reduces the actual sensing area of the PVDF material, which increases the stress of the sensing pillars and therefore generates a larger charge *Q*. Excluding the capacitance of the air between pillars, the design with patterned electrodes further reduces the capacitance *C* of the sensor. According to

$$V_o = Q / C , \tag{1}$$

the output voltage V_o dramatically increases compared with that generated by PVDF film sensors.

We have analyzed three PVDF sensor designs: solid PVDF film, PVDF micro-pillars with full electrodes, and micro-pillars with patterned electrodes. Figure 2 shows the open circuit of a flat PVDF film sensor. The open circuit voltage developed across the film thickness is

$$V_0 = -g_{33} \cdot P \cdot h , \tag{2}$$

where g_{33} is piezo stress constant in the x_3-direction, P is the external applied pressure (here, the stress induced in the material is equal to the pressure) and h is the thickness of PVDF film. The static sensitivity is defined by

$$K_1 = \frac{V_0}{P} . \tag{3}$$

Substitution of Eq. (2) into (3) gives

$$K_1 = -g_{33} \cdot h . \tag{4}$$

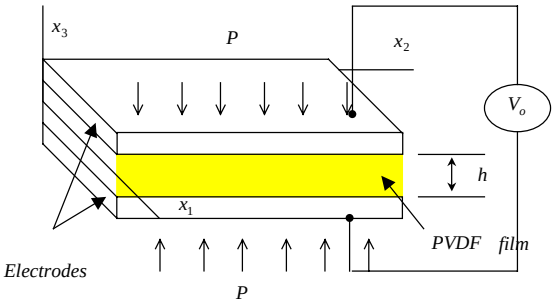

Figure 2. PVDF film open circuit.

For micro-pillars with patterned electrodes (as shown in Figure 1), the stress on each pillar due to the application of normal pressure on the sensor surface is

$$\sigma = \frac{(d+g_1)\cdot(d+g_2)}{\pi d^2/4} \cdot P . \tag{5}$$

The sensitivity of micro-pillars in this case is

$$K_2 = \frac{(d+g_1)\cdot(d+g_2)}{\pi d^2/4} \cdot (-g_{33} \cdot h) . \tag{6}$$

Without loss of generality, we assume $g_1 = g_2 = g$. The sensitivity of the pillar sensors based on patterned electrodes relative to the sensitivity of PVDF film is

$$K_{r2} = \frac{(1+g/d)^2}{\pi/4} , \tag{7}$$

which monotonically increases with the ratio of the gap between pillars and the pillar diameter, g/d . The effect of the air gap between pillars is to increase the stress on the sensing material and therefore to increase the sensor's output voltage and sensitivity.

Figure 3 shows an alternative design in which a film at each sensing side is introduced to form one continuous, flat electrode. The induced charge by the piezoelectric pillars is the same as in the case of patterned electrodes,

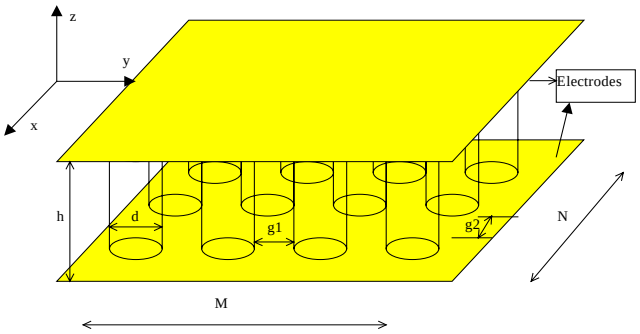

Figure 3. Schematic diagram of PVDF micro-pillar sensor based on full electrodes.

$$Q = Q_p = C_p \cdot V_p, \tag{8}$$

where Q is the total generated charge, Q_p is the charge generated by the micro-pillars, C_p is the total capacitance of the micro-pillars, and V_p is the voltage generated by the micro-pillars. The total capacitance is, by definition,

$$C_p = \varepsilon \cdot \frac{A}{h} = \varepsilon \cdot \frac{M \cdot N \cdot \pi/4 \cdot d^2}{h}, \tag{9}$$

and the voltage is given by

$$V_p = -g_{33} \cdot \sigma \cdot h. \tag{10}$$

Substitution of (5) into (10) gives

$$V_p = -g_{33} \cdot P \cdot \frac{(d+g_1)(d+g_2)}{\pi/4 \cdot d^2} \cdot h. \tag{11}$$

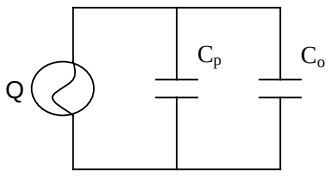

C_p: Pillars capacitance
C_o: Air capacitance

Figure 4. Equivalent circuit of micro-pillar array with full electrodes.

Figure 4 shows the electrical equivalent circuit of PVDF micro-pillars with full electrodes, in which the charge induced by the sensor is distributed between the capacitance of the micro-pillars and the air gap. The total capacitance is the sum of the two capacitances,

$$C_t = C_p + C_o, \tag{12}$$

in which the air capacitance is

$$C_o = \varepsilon_o \cdot \frac{M \cdot N \cdot \left[(d+g_1)(d+g_2) - \pi/4 \cdot d^2\right]}{h}. \tag{13}$$

Since the two capacitances are connected in parallel, the voltage drop is the same across the micro-pillars and air gap,

$$V_o = \frac{Q}{C_t}. \tag{14}$$

Combination of Eqs. (8)-(9) and (11)-(14) gives the sensitivity of PVDF micro-pillars with full electrodes,

$$K_3 = \frac{\varepsilon_r (d+g_1)(d+g_2)}{\pi/4 \cdot (\varepsilon_r - 1) \cdot d^2 + (d+g_1)(d+g_2)} \cdot (-g_{33} \cdot h). \tag{15}$$

As before, the assumption $g_1 = g_2 = g$ gives the sensitivity of the pillar sensors based on full electrodes relative to the sensitivity of PVDF film,

$$K_{r3} = \frac{\varepsilon_r (1+g/d)^2}{\pi/4 \cdot (\varepsilon_r - 1) + (1+g/d)^2}. \tag{16}$$

In this case, the relative sensitivity of the micro-pillar sensor is limited by the relative permittivity of the material, and the upper bound $K_{r3} = \varepsilon_r$ as g/d goes to infinity.

A comparison of the sensitivities relative to the solid PVDF film is shown in Figure 5. The micro-pillar sensor with patterned electrodes theoretically has an unlimited sensitivity with increasing geometry ratio *g/d* (assuming $g = g_1 = g_2$).

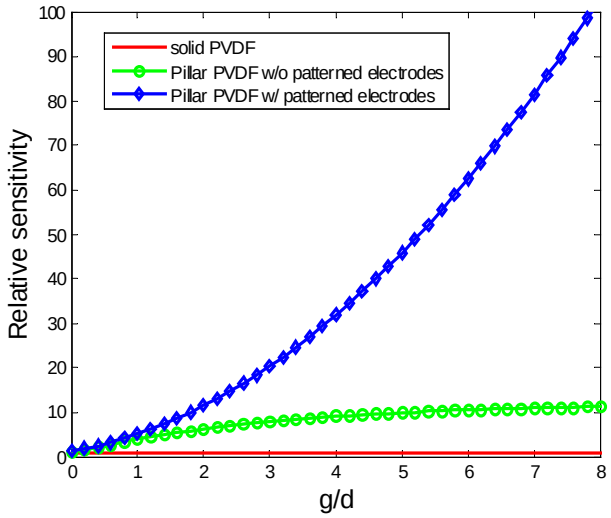

Figure 5. Relative sensitivity of the proposed PVDF micro-pillar sensor with patterned electrodes compared to PVDF film and fully electroded micro-pillars. The gaps are assumed equal ($g = g_1 = g_2$).

To simplify the design of the micro-pillars with patterned electrodes, we neglect the width of the connecting tabs, which is reasonable when the line width of these tabs is relatively small compared to the diameter of each pillar. In practice, the smallest tab width is about 2 microns. If the diameter of micro-pillars is not big enough, this factor needs to be included in the calculation of sensitivity.

Optimization

Nonlinear programming (NLP) techniques are used to find a minimum or maximum of an objective function in N dimensions which satisfies arbitrary complex constraints. Many algorithms have been developed for solving such problems, such as Large-Scale Optimization and Medium-Scale Optimization. The large-scale algorithm is a subspace trust region method and is based on the interior-reflective Newton method described in [8] and [9]. Each iteration involves the approximate solution of a large linear system using the method of preconditioned conjugate gradients (PCG). Usually, the problem can be expressed in the form

$$\begin{cases} \text{minimize} \quad f(x) \\ h_i(x) \le 0 \quad i = 1,\ldots,m \\ g_i(x) = 0 \quad i = 1,\ldots,k \\ l_j \le x_j \le u_j \quad j = 1,\ldots,n \end{cases} \tag{17}$$

Here, x is an N-dimensional list of design variables; $f(x)$ is the objective function; $h_i(x)$ are inequality constraints; $g_i(x)$ are equality constraints; and $l_j \le x_j \le u_j$ are constraints for all design variables.

The functions $f(x)$, $h_i(x)$ and $g_i(x)$ can be any linear or nonlinear combination of the design variables. In this case, a constrained NLP optimization algorithm was developed to obtain the sensor's geometric parameters (M, N, d, g1, g2 and h) needed to achieve 100x the sensitivity of existing commercial sensors, dynamic range up to 181dB, frequency bandwidth of 100 kHz, and millimeter-size footprint. The NLP optimization algorithm was integrated into Matlab.

The design variables that were optimized are M, N, h, d, g1, g2 and R (total input resistance of the amplifier). The design variables can be treated as independent of each other, while the dependent variables are related by the equality constraints. The total input resistance cannot be chosen arbitrarily because the input resistance of the amplifier is usually determined in the datasheet of the product. The height of the pillars is dictated by manufacturing constraints and usually takes integer values such as 10 μm or 20 μm.

For this micro-acoustic sensor design, the main interest is to seek the smallest sensor which achieves a given sensitivity. Therefore, the objective function is to minimize the sensor area, which is expressed by

$$f(x) = M \cdot N \cdot (d + g1) \cdot (d + g2). \tag{18}$$

Bounds on the design variables are affected by the ability of the manufacturing process and amplifier input resistance. For this case, they are defined by

$$\begin{cases} 1 \le M \le 200 \\ 1 \le N \le 200 \\ 1\mu m \le d \le 1000\mu m \\ 1\mu m \le g_1 \le 1000\mu m \\ 1\mu m \le g_2 \le 1000\mu m \\ 1\mu m \le h \le 500\mu m \\ 100M\Omega \le R \le 1T\Omega \end{cases} \tag{19}$$

The constraints are described as follows:

1) Resonance frequency

The basic sensing element, the PVDF pillar, can be modeled as a continuous rod fixed at one end and free at the other end, as shown in Figure 6. Assuming slender rod and ignoring inertial effects, the governing equation for the longitudinal vibrations of a rod has the form

$$\frac{\partial^2 u}{\partial x^2} - \frac{1}{c^2}\frac{\partial^2 u}{\partial t^2} = 0 \tag{20}$$

where u denotes the axial displacement at position x and time t; $c = \sqrt{\frac{E}{\rho_o}}$, where E and ρ_0 are the Young's modulus and mass density of the material, respectively.

According to Eq. (20) and applying fixed-free boundary conditions, one can obtain that the natural frequencies are expressed by

$$\omega_r = \frac{(2r-1)\pi}{2h}\sqrt{\frac{E}{\rho_o}} \quad r = 1,2,3,\ldots \tag{21}$$

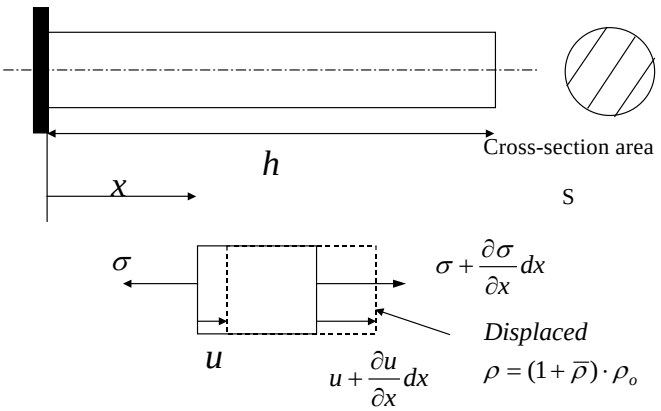

Figure 6. Schematic of a continuum rod model.

A PVDF rod can be divided into a second order system (Figure 7(a)) and a first order system (Figure 7(b)). The system transfer function is expressed by

$$\frac{E_o(s)}{F_i(s)} = \frac{K_1 \tau S}{\tau S + 1} \frac{K_2}{\frac{1}{\omega_n^2}s^2 + \frac{2\xi}{\omega_n}s + 1}, \tag{22}$$

in which τ is the time constant of the first order system, ϖ_n is the natural frequency of the second order system, ξ is damping ratio, K_1 and K_2 are the gains of the first order system and the second order system, respectively.

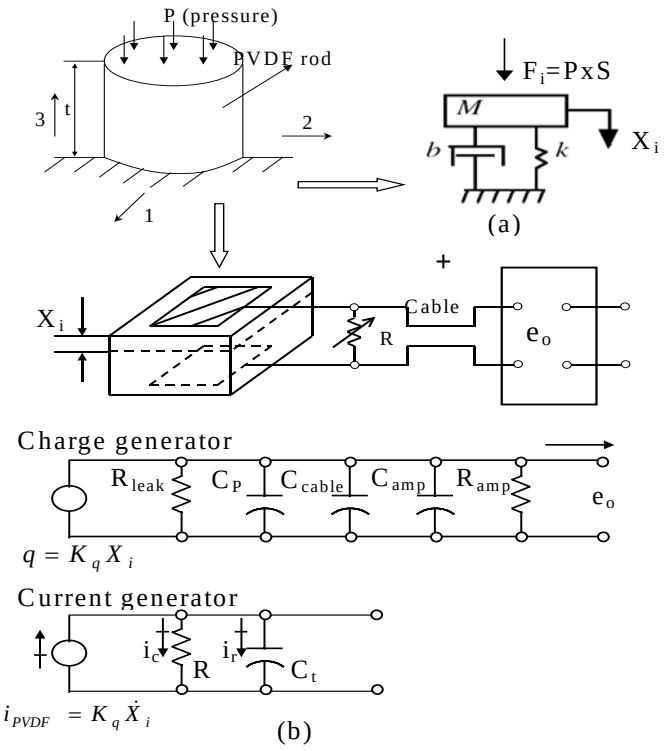

Figure 7. PVDF rod model and equivalent circuit.

The frequency response associated with Eq. (22) is shown in Figure 8. If the sensor is operated in the flat range of the frequency response and the error is ±5%, the bandwidth of the system will be from $3/\tau$ to $\omega_n/5$. The design bandwidth of the acoustic sensor is 20 Hz to 20 kHz, which implies

$$\omega_n/5 \geq 20\times10^3\times(2\pi) \qquad (23)$$

From Eq. (21), the first natural frequency of the PVDF rod (let $r=1$) is

$$\omega_n = \frac{\pi}{2h}\sqrt{\frac{E}{\rho_0}}. \qquad (24)$$

Substitution of Eq. (24) into Eq. (23) and solution for h gives,

$$h \leq 265\mu m, \qquad (25)$$

which represents the natural frequency constraint.

2) Cut-off frequency

According to Figure 8 and the bandwidth requirement, the cut-off frequency constraint is

$$3/\tau \leq 20\times(2\pi). \qquad (26)$$

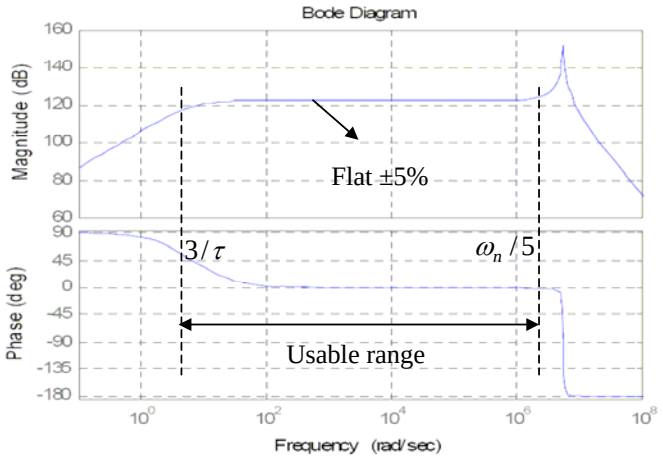

Figure 8. System frequency response.

From Figure 7(b), the time constant is

$$\tau = RC_t. \qquad (27)$$

For the case of micro-pillars with patterned electrodes, the total capacitance of the system is the capacitance of the pillars (note that the capacitance of the cable and the amplifier is relatively small, compared to the capacitance of the pillars), so that

$$C_t = C_p. \qquad (28)$$

Combining Eqs. (9), (28), (27) and (26), one gets that the cut-off frequency constraint is

$$\frac{3h}{R\cdot M\cdot N\cdot\varepsilon\cdot d^2} - 40\pi \leq 0. \qquad (29)$$

Note that for the case of micro-pillars with full electrodes, the total capacitance of the system is the sum of the capacitance of the pillars and the capacitance of air.

3) Dimensional limits in the *x* and *y* directions

The acoustic sensor is designed to be packaged in a millimeter-sized enclosure, which requires that the dimensions in the *x* and *y* directions cannot be greater than a half inch. The dimensional constraints in the *x* and *y* directions thus are:

$$M\cdot N\cdot(d+g1) - 12.7\times10^{-3} \leq 0, \qquad (30)$$

$$M\cdot N\cdot(d+g2) - 12.7\times10^{-3} \leq 0. \qquad (31)$$

4) Sensitivity

Based on the specifications of existing commercial products, the acoustic sensor must have a sensitivity of no less than $0.3V/psi$, i.e. $4.35\times10^{-5}V/pa$. According to Eq. (6), the sensitivity constraint thus has the form

$$4.35\times10^{-5} - (-g33)\cdot\frac{(d+g1)\cdot(d+g2)}{\pi/4\cdot d^2}\cdot h \leq 0. \qquad (32)$$

5) Yield strength

Sound pressure level (SPL) is the measure of the root mean square (rms) sound pressure of a sound relative to a reference value, $20\mu Pa$. The SPL is defined by

$$SPL = 20\log_{10}\frac{p}{20\cdot 10^{-6}}(dB) \qquad (33)$$

The dynamic range of this acoustic sensor is up to 181dB. Therefore, plug this number into Eq. (33), one can get

$$20\log\frac{P\max}{20\cdot 10^{-6}} = 181(dB) \qquad (34)$$

where $P_{\max}$ is the maximal measured pressure. According to the yield strength rule, one can get that the yield strength constraint is

$$P_{\max}\cdot\frac{(d+g1)\cdot(d+g2)}{\pi/4\cdot d^2} \le \sigma_Y \qquad (35)$$

where σ_Y is the yield strength of PVDF.

6) Buckling load

The Euler formula for columns is

$$F_{\max} = \frac{\pi^2 EI}{(rh)^2}, \qquad (36)$$

where F is maximum or critical force (vertical load on column), E is modulus of elasticity, I is area moment of inertia, h is unsupported length of column, and r is column effective length factor. For both ends pinned, r = 1.0; for both ends fixed, r= 0.50; for one end fixed and the other end pinned, r= 0.70; for one end fixed and the other end free to move laterally, r= 2.0.

For the micro-pillar sensor, the buckling load condition is

$$P_{\max}(d+g1)\cdot(d+g2) \le F_{\max}. \qquad (37)$$

Substitution of Eq. (36) into Eq. (37) and considering the area moment of inertia of a round pillar,

$$P_{\max}(d+g1)\cdot(d+g2) - \frac{\pi^2\cdot E\cdot\pi/4\cdot d^2}{(r\cdot h)^2} \le 0. \qquad (38)$$

7) Aspect ratio

Due to limitations of micromolding, the aspect ratio of the micro-pillars usually is no greater than 2,

$$h/d \le 2. \qquad (39)$$

SIMULATION RESULTS AND DISCUSSION

Figures 9-13 show design curves calculated with the optimization procedure described in the previous section. Specifically, the figures show calculations of pillar diameter, pillar gap, g/d ratio, length and aspect ratio vs. pillar height based on different amplifier input resistances, respectively. These plots provide information on the selection of the amplifier input resistances and the pillar height. Figure 9 shows that the calculated optimal pillar diameter monotonically increases with pillar height regardless of the input amplifier resistance values. Figure 11 shows g/d ratio follows the opposite trend. Figure 12 shows that if the amplifier input resistance is greater than $100G\Omega$, the overall footprint of the sensor could be less than $1mm\times 1mm$. However, the aspect ratio of these two cases are greater than those of the other cases, which means that the fabrication ratio must be improved and this is not always feasible.

In addition, according to Figure 13, if the fabrication ability of aspect ratio was 4, any amplifier input resistance (from $1G\Omega$ to $1000G\Omega$) would be suitable. The pillar height should be less than $15\mu m$ if the amplifier input resistance was bigger than $100G\Omega$.

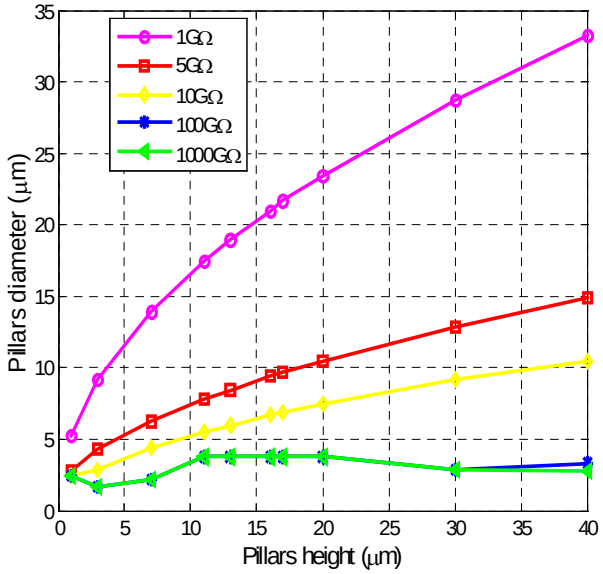

Figure 9. Optimal pillar diameter vs. pillar height as a function of amplifier input resistance.

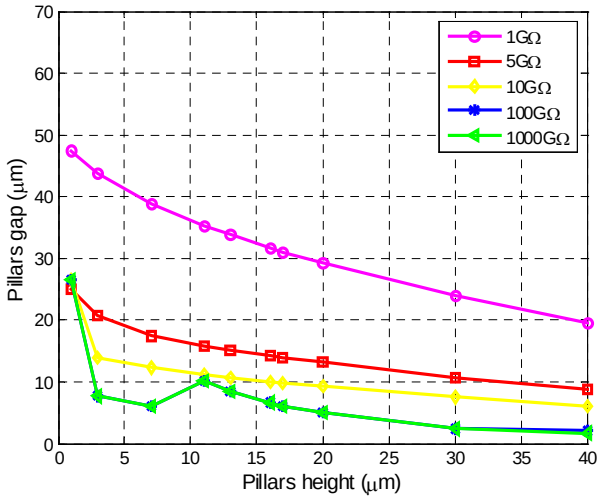

Figure 10. Optimal pillar gap vs. pillar height as a function of amplifier input resistance.

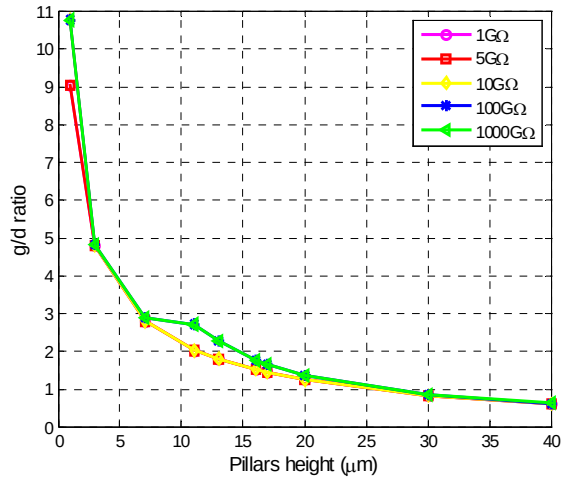

Figure 11. Optimal g/d ratio vs. pillar height as a function of amplifier input resistance.

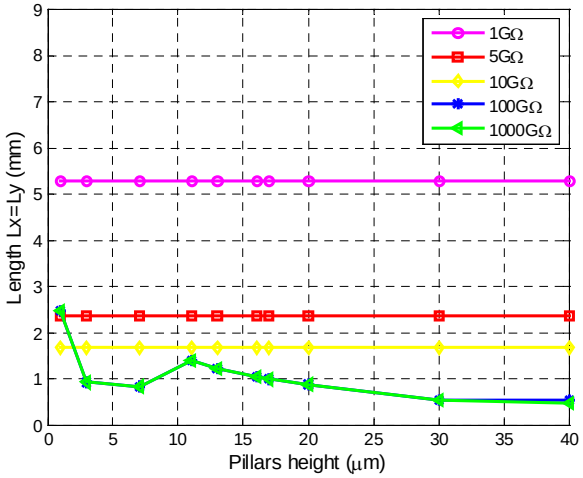

Figure 12. Optimal length vs. pillar height as a function of amplifier input resistance.

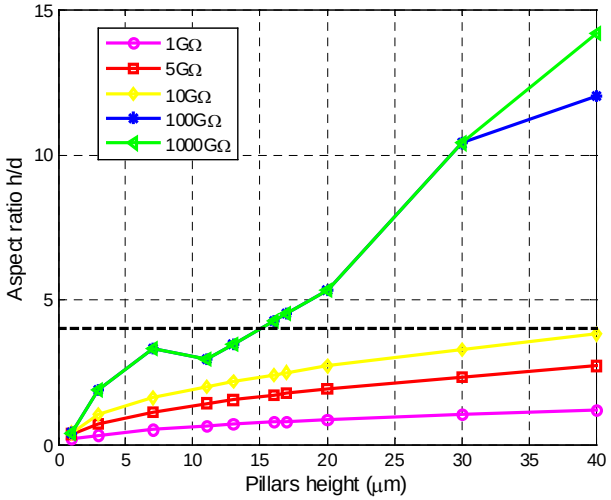

Figure 13. Optimal aspect ratio vs. pillar height as a function of amplifier input resistance.

CONCLUDING REMARKS

This paper presents the design and theoretical analysis of a new type of millimeter-size acoustic sensor that uses Polyvinylidene Fluoride (PVDF) micro-pillars and patterned electrodes. The relative sensitivity analysis shows that PVDF sensors based on micro-pillar arrays and patterned electrodes exhibit much higher sensitivity than commercial PVDF film sensors and micro-pillar arrays with full electrodes, while exhibiting an equally broad frequency bandwidth. A constrained optimization algorithm has been developed as a function of geometric parameters and electrical parameters of the sensor and conditioning amplifier. Simulation results provide guidance for micro-fabrication and amplifier selection.

ACKNOWLEDGMENTS

We are grateful to the member organizations of the Smart Vehicle Concepts Center (www.SmartVehicleCenter.org) and the National Science Foundation Industry/University Cooperative Research Centers program (www.nsf.gov/eng/iip/iucrc) for supporting this work.

REFERENCES

[1] Dargaville, T.R., Celina, M.C., Elliott, J.M., Chaplya, P.M., Jones, G.D., Mowery, D.M., Assink, R.A., Clough, R.L., and Martin, J.W., 2005, "Characterization, Performance and Optimization of PVDF as a Piezoelectric Film for Advanced Space Mirror Concepts," *SANDIA report, SAND2005-6846*,pp. 9-12

[2] Wang, F., Tanaka, M., and Chonan, S., 2003, "Development of a PVDF Piezopolymer Sensor for Unconstrained In-sleep Cardiorespiratory Monitoring," *J. Intell. Mater. Syst. and Struct.*, **14**, pp.185-190.

[3] Fujitsuka, N., Sakata, J., Miyachi, Y., Mizuno, K., Ohtsuka, K., Taga, Y., and Tabata, O., 1998, "Monolithic Pyroelectric Infrared Image Sensor Using PVDF Thin Film," *Sens. Actuators A*, **66**, pp.237-243.

[4] Wang, Z., Wang, C., and Liu, L., 2005, "Design and Analysis of PZT-Based Micromachined Acoustic Sensor with Increased Sensitivity," *IEEE Trans. Ultrason. Ferroelect., Freq. Contr.*, **24**(2), pp. 45-54

[5] Toda, M., and Thompson, M.L., 2006, "Contact-Type Vibration Sensor Using Curved Clamped PVDF Film," *IEEE Sens. J.*, **6**(5), pp. 1170-1177

[6] Lee, L.J., Madou, M.J., Koelling, K.W., Daunert, S., Lai, S., and Koh, C.G., 2001, "Design and Fabrication of CD-like Microfluidic Platforms for Diagnostics: Microfluidic Functions," *Biomed Microdevices*, **3**(3), pp. 245-254

[7] Ferrell, N., Woodard, J., and Hansford, D., 2007, "Fabrication of Micro- and Nanoscale Polymer Structures by Soft Lithography and Spin Dewetting," *Biomed Microdevices*, **28**(8), pp. 966-971

[8] Coleman, T.F. and Li, Y., 1996, "An Interior, Trust Region Approach for Nonlinear Minimization Subject to Bounds," *SIAM Journal on Optimization*, **6**, pp. 418-445

[9] Coleman, T.F. and Li, Y., 1994, "On the Convergence of Reflective Newton Methods for Large-Scale Nonlinear Minimization Subject to Bounds," *Mathematical Programming*, **67**(2), pp. 189-224